Note: this non-peer reviewed preprint. It has been submitted to a peer-reviewed journal for publication.

Machine learning predictions of summertime warming jumps on decadal timescales

Emily M. Gordon[1,2,*] **and Noah S. Diffenbaugh**[2]

[1]Department of Physics, University of Auckland, Auckland, New Zealand
[2]Doerr School of Sustainability, Stanford University, Stanford, USA
[*]Author to whom any correspondence should be addressed.
emily.gordon@auckland.ac.nz

Abstract. Extreme events are responsible for some of the most severe impacts of climate change, but regional extreme event prediction remains a challenge as the events contain a large amount of stochasticity. Here we demonstrate an approach for predicting future summertime temperature extremes on decadal timescales by first identifying an abrupt jump in average summertime temperature as a covariate of extreme summertime temperatures, and then showing that these jumps can be predictable. We train a convolutional neural network (CNN) on historical and future global climate simulations to predict a confidence that future five-year mean summertime temperatures will jump above a hot threshold given maps of recent sea surface temperature variability and the global warming level. We show that in most land regions, the CNN outperforms a classifier that relies solely on the forced temperature response, implying that information about the prior 10-year SST variability improves the CNN's prediction skill and confidence. We input the observational record into the CNN as independent unseen data and observe some skill, with investigation revealing that this skill is driven by the CNN learning conditions that best suppress summertime temperature jumps. Our study emphasizes the importance of targeted methodology for diagnosing extreme event predictability, and demonstrates that future predictions of extremes can be improved by considering the prior 10-year SST variability, rather than just the forced response to global warming.

1. Introduction

Climate change is causing mean state changes in the climate system, including increases in temperature and atmospheric water vapor, accompanied by increases in the frequency and intensity of extreme climate events [Meehl et al., 2000; Fischer et al., 2021; Seneviratne et al., 2021]. Extreme events are among the most directly harmful and costly aspects of climate change, evident through their effects on human health, agriculture, and critical infrastructure [Ebi et al., 2018; Field et al., 2012; White et al., 2023]. Predicting regional extreme events on actionable timescales is therefore crucial for climate change adaptation planning [Dunstone et al., 2022]. Climate models can be used to examine the distribution of possible changes in the frequency of extreme events for particular levels of warming [Seneviratne et al., 2021]. However, it is difficult to accurately predict the occurrence of extreme events on multi-year timescales beyond the average increase we expect from climate change [Eade et al., 2012; Delgado-Torres et al., 2023], and forecast skill for an extreme in regional monthly average temperatures likely lasts no longer than a year after forecast initialization [Becker et al., 2013]. This difficulty arises because specific combinations of oceanic, land surface and meteorological conditions are required for an extreme event to occur on top of the background warming trend [Trenberth et al., 2015; Rupp et al., 2017]. These natural variations in the climate system, often called "internal climate variability", dominate the uncertainty in future climate outcomes on 5-10 year timescales, particularly on regional spatial scales [Hawkins and Sutton, 2009; Lehner et al., 2020]. To accurately predict the probability or occurrence of an extreme event therefore requires identifying and predicting the shifts in internal variability that are most likely to lead to a regional extreme event.

Approaches to investigating predictable variability traditionally involve generating a hindcast ensemble of the historical record by initializing a global climate model (GCM) to an approximate estimate of prior climate states, and evolving the GCM forward to examine how well its prediction captures prior variability. These initialized forecasts can be compared with an accompanying "uninitialized" ensemble of the historical period to examine what predictive skill is attributable to the GCM's initialization (i.e. how well it captures near-term internal variability) or merely to the GCM correctly predicting the climate response to historical anthropogenic emissions [Boer et al., 2016; Meehl et al., 2021]. While these methods show power in understanding predictability particularly in the ocean, it is more difficult to quantify the predictability of extreme events because they are by definition rare. Furthermore, initialization biases a GCM away from its climatology, leading to unphysical behavior for the first years of an integration (which must be corrected) [Meehl et al., 2022]. Evidence also suggests that GCM hindcasts inherently contain an unrealistically low fraction of predictable variability, though the causes are debated [e.g., Eade et al., 2014; Smith et al., 2019; Zhang and Kirtman, 2019]. Thus, while prior investigation of the predictive skill of extreme temperature and precipitation attribute much skill to the GCM correctly predicting the response to greenhouse gases in the historical period [Delgado-Torres et al., 2023], this is likely a lower estimate for the predictable variability in the real climate system.

Continued hope for decadal prediction of extreme events lies in more tailored methodologies which take hypothesis-based approaches to test the predictability of climate conditions that may best constrain the likelihood of some indicator of climate extremes. For example, by linking the probability of temperature extremes to an atmospheric Rossby wave pattern driven by sea surface temperature variability in the North Atlantic Subpolar Gyre, Borchert et al. [2019] demonstrate the potential skill in predicting decadal variability in heat extremes over Europe. Across the globe, extreme events have been linked to large-scale shifts

arising from natural variability. For example, Sahel drought has been linked to Atlantic SST variability contributing to a shift in the background climate to a warmer and drier regime [He et al., 2022]. Basin-wide oceanic variability in the Pacific ocean likely contributes to extreme precipitation in East Asia, Australia, and North America[Wei et al., 2021], while summertime heat extremes over Northern Hemisphere land regions have been linked to developing El Nino Southern Oscillation (ENSO) conditions [Arblaster and Alexander, 2012; Luo and Lau, 2020]. Theoretically, a large-scale shift in internal variability may therefore coincide with an abrupt increase in the risk of experiencing an extreme event.

Recent innovations in machine learning have by-passed the issues of initialization shock and underestimated predictable variability that are inherent to GCM hindcast ensembles. By directly training machine learning models on GCM data, and using the trained models to predict the observational record, prior work has shown that there is predictable internal variability in the ocean throughout the observational period. Notably, while trained on imperfect climate model data, these machine learning models are able to capture predictable variability in the observed historical record, even though observations are "unseen" by the trained models [Davenport et al., 2024; Gordon and Diffenbaugh, 2025]. Further research investigating predictability in GCMs under elevated greenhouse gas forcing demonstrates that internal variability still provides a substantial fraction of predictable variability [Gordon et al., 2023], implying that future greenhouse gas forcing will not immediately overwhelm the potential predictive skill provided by internal variability.

In this study, we design a machine learning-based method for predicting a covariate of an extreme heat event on multi-year timescales: We hypothesize that an abrupt jump in regional average summertime temperatures coincides with an enhanced likelihood in the occurrence of a multi-day heat event, because when the underlying temperature distribution is shifted warmer, extreme events are more likely to occur. We also hypothesize that, because summertime temperature variability is tied to large-scale, low frequency internal variability [Arblaster and Alexander, 2012; Luo and Lau, 2020], jumps in average summertime temperatures over a multi-year period can be predictable. Therefore, we first verify that jumps in average regional summertime temperatures coincide with a local increase in the likelihood of experiencing a multi-day temperature extreme in GCM data. Then, motivated by the success of prior studies using machine learning to predict climate variability on multi-year timescales, we examine the predictability of such summertime warming jumps in both GCM output and historical reanalysis using a convolutional neural network.

2. Materials & Methods

2.1. Global Climate Model (GCM) data

We use GCM data from multiple large single-model ensembles, along with their associated future warming scenarios (see Table 1). We select large ensembles with at least 25 members in both the historical period (from at least 1920 onwards) and a corresponding future warming scenario to enable training the neural networks across many realizations of the physical climate system under historical forcing and scenarios of the future. The GCMs were chosen as those that matched these criteria. We use up to 30 members to avoid over-representing any one GCM in the CNN training and results. We also combine SSPs in the training set to allow the CNNs to see a diverse representation of the future climate. We examine the CNN's performance on each specific GCM and corresponding SSP in section 3.4.

We use sea surface temperature (SST) bilinearly regridded to $4^\circ \times 4^\circ$ resolution, and

Table 1. Individual GCMs with their associated climate change scenarios, variables, number of members used, and citation.

GCM	SSP	Variables	Number of members used	Reference
ACCESS-ESM1-5	SSP 2-4.5	tas, tos	30	Ziehn et al. [2020]
CanESM5	SSP 5-8.5	tas, tos, tasmax	25	Swart et al. [2019]
CESM2	SSP 3-7.0	tas, tos, tasmax	100	Rodgers et al. [2021]
GFDL-SPEAR	SSP 5-8.5	tas, tos, tasmax	30	Delworth et al. [2020]
MIROC6	SSP 5-5.5	tas, tos, tasmax	30	Tatebe et al. [2019]
MPI-ESM1-2–LR	SSP 5-8.5	tas, tos, tasmax	30	Olonscheck et al. [2023]

2 m air temperature averaged to $10° \times 10°$ degree boxes for land grid points. Grid points with greater than 20% ocean coverage are not considered land points. We also calculate the global mean temperature (GMT) anomaly within each ensemble member by first calculating the annual mean timeseries of global area-weighted 2 m air temperature, and then subtracting that particular ensemble member's 1920-1950 GMT mean. We take this period as our baseline, rather than the conventional 1850-1900 pre-industrial period, as GFDL-SPEAR does not provide the full historical timeseries. We choose to generate the anomaly timeseries for each member individually so that the CNN learns to treat each member as an independent realization of the climate system. This choice means that observations can be easily incorporated as an out-of-sample testing set as there is only one realization of the observational record.

Additionally, we quantify the effect of summertime warming jumps on experiencing multi-day average maximum temperature that exceeds recent extremes using daily maximum and monthly mean near-surface temperatures from all 100 members of the CESM2 large ensemble. For the daily maximum temperatures, the data are bilinearly regridded to $5° \times 5°$ resolution and then a 3-day rolling mean is applied. We then calculate the annual maximum 3-day temperature at each grid point in each ensemble member. We define that a five year period includes a 3-day heat event if that five-year period contains a 3-day average maximum temperature that exceeds any 3-day average maximum temperature from the preceding 10-year period. We also examine the co-occurrence of CNN predictions of summertime warming jumps with 3-day heat events in GCM large ensembles. (Note that daily maximum temperature was not accessible for all members of the ACCESS-ESM1-5 large ensemble so it is excluded from this analysis; Table 1). We first average the GCM large ensemble data to a regular 10×10 grid over the land surface. We then calculate the annual maximum 3-day average maximum temperature, and classify a 3-day heat event using the above definition (i.e., a heat event occurs if a 3-day maximum temperature in a five year period exceeds any 3-day maximum temperature in the prior 10 year period).

2.2. Observations & Reanalysis

We use 2 m air temperature from the ERA5 reanalysis from 1940 to 2024 [Hersbach et al., 2020] to validate the CNN predictions in the observed climate. As with the GCM data, 2 m temperatures are averaged to $10° \times 10°$ boxes over land surface regions, with grid points with

greater than 20% ocean coverage not considered. While ERA5 data quality can be impaired prior to the satellite-era, we use large spatial ($10° \times 10°$) and temporal (5 year summertime) averaging which reduces some of the biases.

As ERA5 data are not available prior to 1940, we compute the global mean temperature timeseries using HadCRUTv5 and the recommended method [Morice et al., 2021] (i.e., computing annual mean area weighted global mean from the provided anomaly data, adding the annual mean global mean 1961-1990 climatology, and then subtracting the 1920-1950 annual mean global mean such that the anomaly timeseries is consistent with that from the GCM data). Finally, for SST observations, we use SST from ERSST from 1940 to 2024 [Rayner et al., 2003], bilinearly regridded to $4° \times 4°$.

2.3. Summertime Warming Jumps

We define a summertime warming jump as an anomalous increase in regional summertime average 2 m air temperature relative to that region's prior ten year average. Because this definition is based on the difference between two consecutive periods in the local temperature timeseries, it accounts for the recent warming experienced in a region. For each year at each grid point, we calculate ΔT as the difference between average summertime temperature for the prior ten years and the next five years ($\Delta T = \bar{T}_{\text{next5summer}} - \bar{T}_{\text{prior10summer}}$). In this study, we determine a jump to have occurred for year y if ΔT exceeds the 90th percentile of all summertime ΔT in the recent historical (1960-1990) period. Note this baseline calculation includes 31 jumps, so the first jump is for 1960, which is calculated as $\Delta T_{1960} = \bar{T}_{1960-1964} - \bar{T}_{1950-1959}$ and hence the baseline calculation includes 1950 to 1994. This threshold is calculated for each individual grid point, climate model and ensemble member. Following convention, summertime is defined as June-July-August in the Northern Hemisphere and December-January-February in the Southern Hemisphere.

Figure 1a demonstrates summertime mean temperatures for Eastern Australia in ERA5, with dots on the timeseries indicating times where a jump occurs. The grid-point-level jump threshold averaged across all GCMs and members is shown in Figure 1b, demonstrating that jump thresholds are lower for regions with lower amplitude interannual temperature variability such as the tropics, and higher over midlatitude land regions where summertime temperatures have higher amplitude interannual variability.

2.4. Convolutional Neural Networks (CNNs)

We train convolutional neural networks (CNNs) to predict the likelihood of a future jump in average summertime temperature (Figure 1c). The architecture used here is largely based on that from Davenport et al. [2024], which similarly used SST from a range of GCMs to make categorical predictions on future decadal variability, with an update to the final dense layers to incorporate the GMT input (see below). A CNN takes images of the annual mean SST for each of the prior ten years (10 maps in total) as inputs. To standardize each set of inputs, the average SST map is calculated for the set of 10 maps, and this average map is subtracted from each of the individual annual mean maps, so that each grid point for each individual input map is its anomaly from the 10 year mean. We choose this method so that each input sample is not dependent on full GCM statistics, nor does it require information about the true forced climate response, but the inputs still contain recent SST variability. Note we do not include additional standardization, as this did not improve neural network performance (Figure S1), nor did latitude weighting on the input SST maps (Figure S2). The

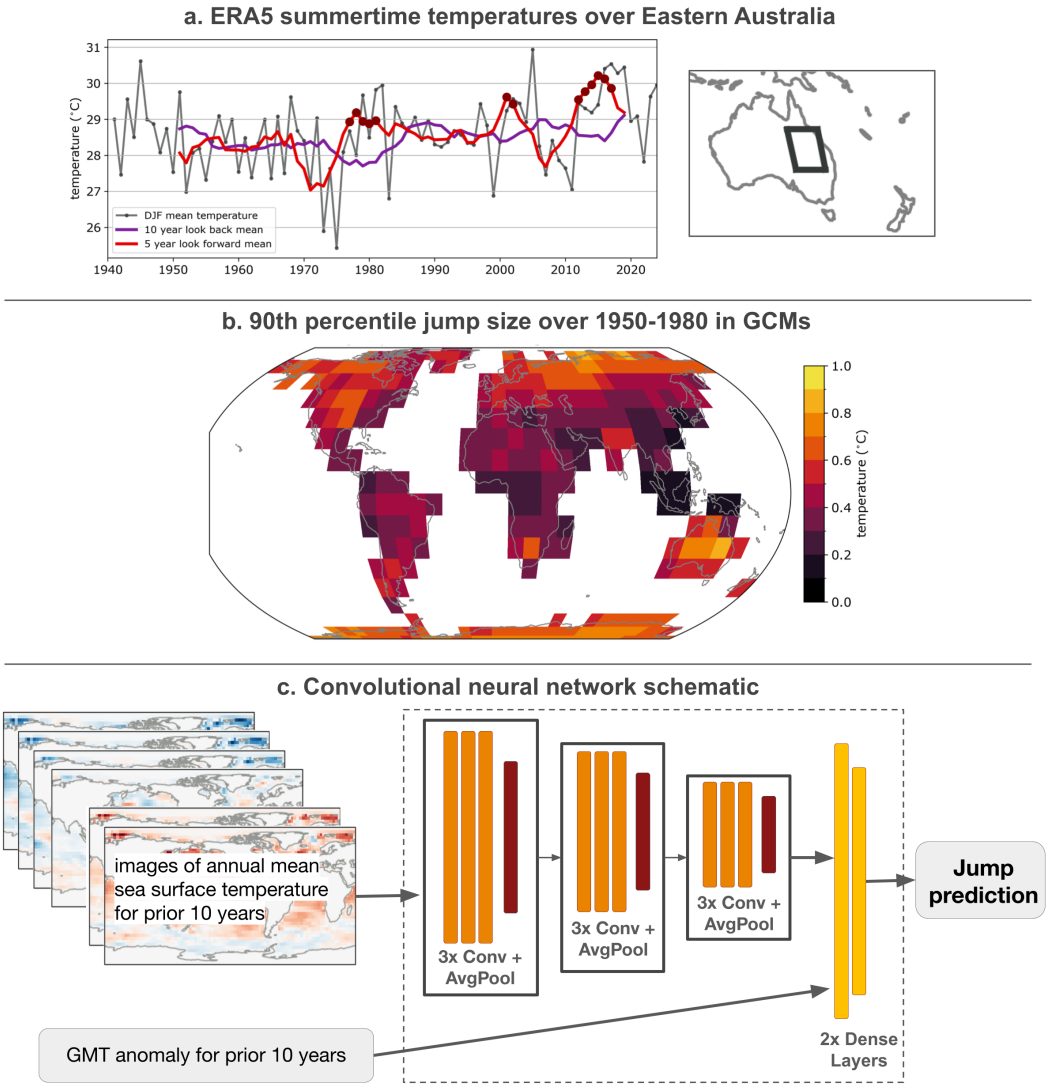

Figure 1. a. Summertime temperatures in Eastern Australia in ERA5 (grey line). 10 year look back mean is in purple and 5 year look forward mean is in red. Dots indicate where the difference between five year future summer temperature (red) and 10 year prior summertime temperature (purple) exceed the jump threshold and therefore are defined as a summertime temperature jump. b. Size (in °C) of the average jump threshold at each grid point, defined as the 90th percentile jump size from 1950-1980, averaged across all GCMs and all members. c. CNN schematic, 10 maps of prior 10 year SST are in put into three sets of convolution-pooling blocks and then passed to a dense layer. The prior 10 year average GMT anomaly is also added at the dense layer. This layer is connected to the output layer which outputs a predicted confidence that a jump will occur

input SST maps are passed through 3 convolutional blocks, each consisting of 3 convolutional layers of 16 filters with a 3×3 kernel, followed by a 2×2 average pooling layer. The final convolutional block is connected to a dense layer of 50 nodes followed by an additional dense layer of 10 nodes. At the first dense layer, the average global mean near-surface temperature (GMT) anomaly of the prior 10 years is also input. The CNN output layer is two nodes with a softmax activation function such that it outputs a predicted confidence that a jump in average summertime temperatures for a specific region will occur.

In total, 10 CNNs are trained for each output grid point with a different random seed and a randomized subselection of GCM ensemble members into training and validation data sets. For analysis, at each grid point we select the three CNNs with the highest accuracy on their respective validation sets. Fifteen members of each GCM large ensemble are used for training, eight for validation and the final seven are kept as independent testing members (except for CanESM5, which only has two testing members due to its smaller ensemble size; Table 1).

The CNNs are trained for up to 200 epochs using categorical cross entropy loss and a batch size of 128 using the stochastic gradient descent optimizer and early stopping when validation loss does not decrease for 20 consecutive epochs. The initial learning rate is 0.01, which decreases by a factor of 10 every time the validation loss does not decrease for 10 consecutive epochs. Training time for all 10 CNNs for all global land grid points takes approximately 8 hours of wall clock time on a single NVIDIA A100 GPU.

3. Results

3.1. Summertime warming jump as a co-variate of an extreme heat event

While the frequency of extreme heat events increases in response to global warming, these events are difficult to predict beyond weather timescales, because they require specific weather conditions (e.g. atmospheric blocking) to occur on top of climate conditions (e.g. anomalous SST warming and/or soil drying). We therefore begin by examining how a jump in summertime warming affects the likelihood of experiencing a local 3-day heat event. In Figure 2a, we show, from the CESM2 large ensemble, the probability that a 3-day heat event in a future five year period exceeds any 3-day heat event that occurred in the prior ten years. This frequency is calculated across all years from 1950-2090, and all ensemble members, meaning that it includes the climate change signal. We see highest likelihoods over the tropics, indicating that in regions where the climate change signal provides a larger fraction of the timeseries variance the likelihood of year-on-year extreme events is higher.

To examine how jumps in summertime warming affect short-term extreme event probability, we quantify the probability that, in the next five years, a 3-day event occurs that exceeds any event from the prior ten years *given* that summertime temperatures jump by the 90th percentile of the historical distribution (Figure 2b). Here we see that the probability of experiencing a 3-day heat event is increased at all grid points, implying that the abrupt warming of summertime temperatures often coincides with increased likelihood of a 3-day heat extreme. We plot the difference between these frequencies in Figure 2c, with positive values showing where a summertime warming jump coincides with an increase in likelihood of a 3-day heat event. In testing for statistical significance, we see that summertime warming jumps significantly coincide with an increased likelihood of experiencing a 3-day heat event at effectively all land surface grid points. While it is perhaps not surprising that a jump in summertime average temperatures coincides with enhanced probability of experiencing an extreme heat event, we have identified a co-variate that is potentially more predictable than

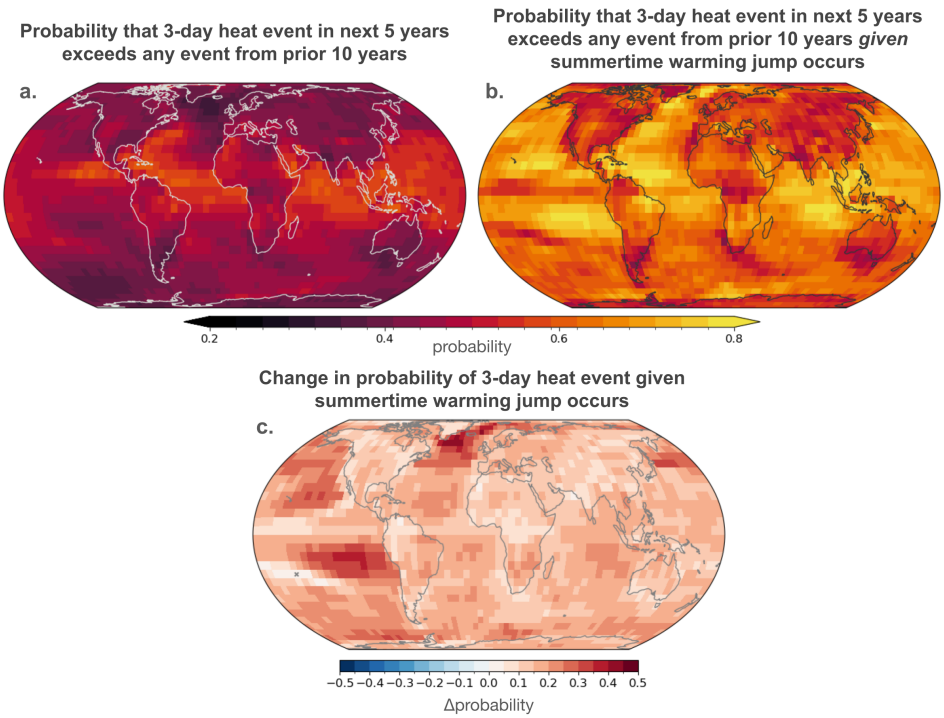

Figure 2. a. Probability that a 3-day heat event in the next 5 years exceeds any from prior 10 years in the CESM2 large ensemble from 1950-2090. b. Probability of that 3-day event occurring given that a summertime warming jump occurs. c. Change in the probability of the 3-day event given summertime jump occurs (i.e. b.-c.). We bootstrap probabilities for each grid point and ensemble member by randomly selecting years from each ensemble member that match the number of jumps in that member and counting the number of 3-day events that occur, repeating this process 1000 times. Stippling indicates where the likelihood increase provided by the summertime warming jump is not distinguishable from bootstrapped frequencies at the 95th percentile.

a 3-day heat event itself. Finally, we expect that the increasing trend in warming due to greenhouse gases will explain some of the relationship between summertime warming jumps and heat extremes. Therefore, we further separate the extreme event frequency into different levels of GMT to control for the greenhouse warming level (Figure S3). We find that this result holds, even at low GMT anomalies (i.e., $0° - 1°$C), implying that this result is not merely a result of both variables increasing in frequency in the future climate.

3.2. Global summertime jump prediction skill

Having found that regional summertime warming jumps are accompanied by an enhanced probability of experiencing a 3-day heat event, we now examine the predictability of such events using convolutional neural networks. We calculate the CNN skill at predicting summertime warming jumps at each $10° \times 10°$ land region (Figure 3a). We use accuracy to quantify CNN skill, which is defined as the number of correct predictions divided by the total number of predictions, with accuracy value of 1 meaning all samples are correctly predicted. We see higher skill in regions with a higher climate change signal relative to the local amplitude of internal variability. For example, the tropics have relatively little year-to-year temperature variability outside of the warming trend and therefore future summertime temperature jumps

that exceed historical variability are more likely with increasing warming. Here the predicted outcome, summertime warming jump, increases in frequency with increasing GMT (as jumps become more likely with steeper warming), so much of this skill likely derives from the CNNs learning the relationship between global mean temperature change and frequency of summertime temperature jumps.

We therefore examine the CNN skill attributable to just learning the GMT response, using permutation importance. This method is a machine learning explainability method that probes the effect of a specific predictor on the machine learning model's outcome [McGovern et al., 2019; Gordon et al., 2023]. We are interested in the effect of the recent SST variability information on prediction skill, so we randomly shuffle the order of the SST input sample maps (i.e. keep each set of 10 the same, but shuffle the order they appear in the test set) while keeping the GMT information in place, and input this information into the CNN. We repeat this process 1000 times to compute the range of predicted outcomes for the randomized SSTs. The average prediction across the range is taken to be the "GMT-only" prediction and we calculate the accuracy of the GMT-only information at each grid point (Figure 3b). The GMT-only prediction skill map demonstrates that much prediction skill can be derived from the response of jump probability to greenhouse gas warming, particularly in regions where the signal of the forced response is much greater than the signal of internal climate variability (e.g., the tropics). To estimate the effect of including recent SST variability as a CNN input on the correct prediction of summertime warming jumps, we take the difference between the CNN accuracy with all input information and the GMT-only accuracy (Figure 3c). Here we plot the percentage increase in accuracy provided by SST variability, demonstrating that much of the land surface shows modest but robust increase in accuracy, particularly over the Amazon basin, the Sahara Desert, and much of Central and West Asia. This increase in accuracy suggests that in many regions, summertime temperature jumps can be predictable beyond the average effect of greenhouse warming.

To probe whether the CNNs have discerned samples that make summertime warming jumps more predictable, we take a "windows of opportunity" approach [Mariotti et al., 2020; Mayer and Barnes, 2021] by examining the CNN's skill based on its prediction confidence. Because the CNN is trained with cross-entropy loss, a CNN's prediction can be interpreted as its confidence in the outcome, with higher values indicating higher confidence. At each grid point, we identify the 20% of samples that are most confidently predicted by the CNN and calculate the CNN's accuracy (Figure 3d). We find that the CNN's skill for its confident predictions is considerably higher than across the full test set, indicating that the CNN has learned the input combinations that are most likely to lead to predictable outcomes.

Given that there is some skill garnered from learning the relationship between jump probability and GMT (Figure 2b), we use permutation importance to test whether the skill enhancement from CNN confidence in Figure 3d is attributable to the CNN confidently learning the forced response. The GMT-only predictions used to generate Figure 2b all have an associated CNN confidence. Therefore, we test whether enhanced CNN confidence, and therefore CNN prediction skill during windows of opportunity, is merely due to the CNN learning the response to GMT warming. We take the 20% most confident samples from the GMT-only predictions and calculate the CNN accuracy for these samples, which reveals the enhancement in CNN skill possible from GMT alone (Figure 2e). We also calculate the percentage difference in accuracy between the 20% most confident samples for all predictions, and GMT-only predictions (Figure 2f). Here, we find increases in accuracy that are attributable to the SST input information over much of the globe. In addition, these increases are generally more substantial than the accuracy increases due to SST information

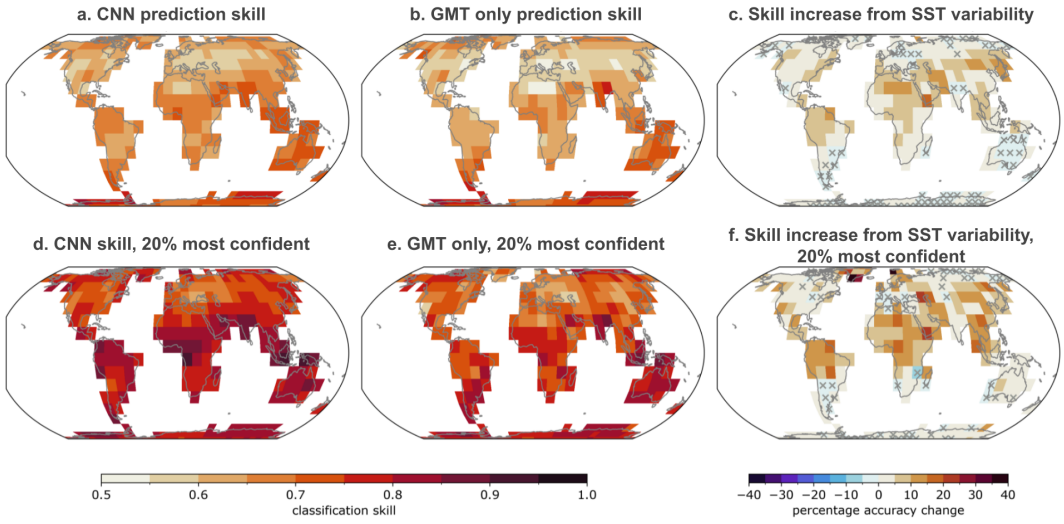

Figure 3. a. CNN accuracy at predicting summertime temperature jumps across all testing samples and grid points. b. Prediction accuracy when only the GMT input provides prediction information. c. Percentage difference between total CNN accuracy and GMT only accuracy (i.e., a.-b.). x indicates grid points where difference is not statistically significant at 95% confidence. d. CNN accuracy in testing samples for the 20% of samples the CNN ranks as most confident. e. CNN accuracy on its 20% most confident predictions when only given GMT information. f. Percentage difference between CNN's most confident predictions and GMT only confidence. x indicates where difference is not statistically significant.

across all testing samples in Figure 2c. These accuracy increases suggest that recent SST information plays a crucial role in predicting summertime warming jumps, and that there are particular SST samples that heighten the CNN's confidence even more than the effect of increased GMT.

3.3. Precision and Recall

One potential concern is that the CNNs learn to only predict the most common class, and in particular that its most confident predictions are only for non-jump samples as that class is more represented in the training data. We verify that the CNNs learn to balance their predictions of the two classes by examining the precision and recall of each class at each grid point for all predictions (Figure S4), and the 20% of samples assigned the highest confidence by the CNN (Figure S5). Precision is calculated for each class by taking all the predictions of a single class and calculating the ratio of correct predictions to all predictions. Recall is calculated by taking all the true samples for a single class and calculating the ratio of correct predictions to true samples. We find that the CNNs have good precision (> 0.5) across almost all grid points for both classes, implying that a predicted output is more likely to be correct than not correct (Figure S4a and S4b). Recall for "no jump" predictions is also strong, implying that these events are well captured (Figure S4c). Recall for "jump" predictions is more variable, with poor recall in the poles and over Australia, suggesting that in these regions much of the CNN skill is driven by learning the "no jump" class (Figure S4d).

We find that almost all precision and recall scores are improved for each class when we consider the samples to which the CNN assigns the most confidence (Fig. S3), implying that

both classes are better predicted with increasing confidence at most grid points. Land grid points where precision is a "NaN" value indicate regions where the CNN never confidently predicts that class. For example, points in Central Africa and the Himalaya region are never confidently predicted as "no jump", and points in the Polar Regions, South Central United States, and Australia are never confidently predicted as "jump". This behavior reveals that, while jumps are likely to become predictable in a future climate, there are regions where they remain unpredictable, likely because the underlying mechanisms do not provide predictability on multi-year timescales.

3.4. Individual GCM Skill

Because the CNNs are trained on multiple GCMs, we can examine how summertime jump predictability varies across the different GCMs (Figure 4). As before, prediction skill is largest in areas where the climate change signal provides a larger fraction of year-to-year variability, and therefore where warming leads to a larger likelihood of near-term temperature increases above historical levels, e.g. the tropics and Arctic (Figure 4, left-hand column). Skill varies widely across the midlatitudes indicating different fractions of predictable variability in the GCMs. For example, North America is well-predicted in ACCESS-ESM1-5 (Figure 4a), while West Africa is best predicted in CESM2 (Figure 4b) and CanESM5 (Figure 4f).

We quantify the role of greenhouse gas warming in summertime jump predictability in each individual GCM, again using permutation importance. To account for the trend information that is unique to a specific GCM and scenario, only samples within a single GCM ensemble are permuted. The skill maps and differences are plotted in the middle and right-hand columns of Figure 4. Once again, we see different amounts of added skill in the different GCMs. While ACCESS-ESM1-5 and CanESM5 show broad regions of skill in the Northern Hemisphere midlatitudes, CESM2, GFDL-SPEAR and MIROC6 exhibit less skill, and MPI-ESM1-2-LR shows little skill anywhere. These GCMs span different climate sensitivities, with CanESM5 and CESM2 exhibiting high sensitivity , ACCESS-ESM1-5 and GFDL-SPEAR exhibiting medium sensitivity, and MIROC6 and MPI-ESM1-2-LR exhibiting relatively low sensitivity [Meehl et al., 2020]. Therefore, while the highest sensitivity GCM shows some of the best skill and the lowest sensitivity shows the worst, there is significant skill in GCMs with more moderate climate sensitivity. Moreover, the ACCESS-ESM1-5 ensemble uses the SSP2-4.5 scenario, which has the lowest radiative forcing of the scenarios used here. Lower forcing implies that there is a smaller climate change signal and yet the CNN performs well in large swaths of the Northern Hemisphere midlatitudes in ACCESS-ESM1-5. Combined, this evidence suggests that while GCM sensitivity to forcing may affect summertime jump prediction skill, significant skill is garnered from unforced SST variability.

We further test the CNN's dependence on the GCMs included in the training set by training an additional set of CNNs, but without MPI-ESM-1-2-LR in the training set. We choose to omit MPI-ESM1-2-LR because the CNN performance is poorest on the MPI-ESM1-2-LR testing members (Figure 4e). However, when MPI-ESM1-2-LR is left out from the training set, the CNNs show degraded skill in the observational record (Figure S6). Therefore, while individual GCMs may not appear to significantly enhance a CNN's skill, it is likely still beneficial to include this data in the training set to aid generalizability on out-of-sample data. This finding aligns with prior work identifying that leaving out GCMs, even those with poor testing performance, does not detrimentally affect the performance of the machine learning model on other GCMs or observations [Gordon and Diffenbaugh, 2025].

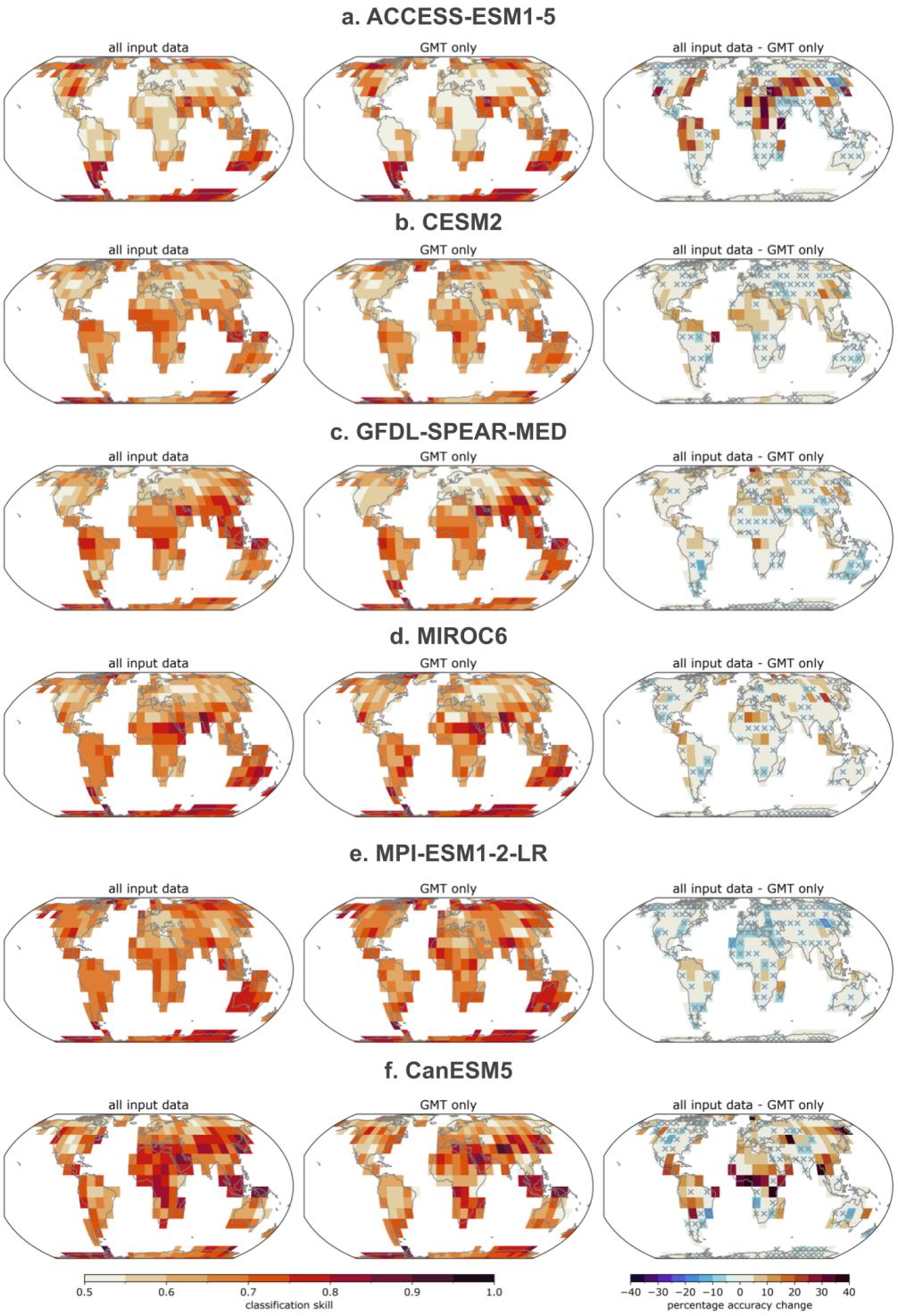

Figure 4. Accuracy in predicting summertime warming jumps in the individual GCMs used in CNN training. Each row is a different GCM, from top to bottom: ACCESS-ESM1-5, CESM2, GFDL-SPEAR, MIROC6, MPI-ESM1-2-LR, CanESM5. Left-hand column is the CNN skill for all testing samples within a GCM. Middle column is GMT-only accuracy for samples within the specified GCM. Right-hand column is the percentage difference between the left-hand and middle columns, showing the percent change in accuracy provided by SST input information. x indicates grid points where the change is not statistically significant at 95% confidence.

3.5. Detecting Heat Events

We examine the CNN's jump prediction as an analog for predicting three day heat events. First, we calculate the likelihood of occurrence of a three day heat event in a future five year period in the testing members of each GCM large ensemble (Figure 5, left-hand column). Then, we calculate the likelihood that the CNN's prediction of a warming jump coincides with the occurrence of a three-day heat event (Figure 5, middle column). That is to say, given that the CNN predicts a warming jump, we calculate the number of heat events that occur. The difference in the frequency of three day heat events and the events detected by the CNN is shown in the right-hand column of Figure 5, with grid points where the CNN's predictions do not outperform random sub-sampling at 95% confidence marked by an "x". The CNN's predictions largely provide enhanced likelihood in detecting a three-day heat event, particularly in the equatorial region, which is a region where most CNN's outperform a GMT only model (Figure 4), implying that the enhanced skill is due to more than just the increasing frequency of heat events with increasing GMT. There are also regions of enhanced detection across the midlatitude continental regions (e.g. North America and East Asia) in most GCMs, which also correspond to increased CNN skill above the GMT-only predictions. The enhanced likelihood of detection of three-day heat events provided by the CNN's summertime jump prediction demonstrates that a summertime warming jump is a key, predictable, indicator of future climate extremes.

3.6. Skill in the Observational Record

To examine if the CNNs have learned realizable real-world predictability, we input observed SST and GMT anomalies into the CNNs trained across all GCMs. For verification data, we use temperature jumps in the ERA5 reanalysis record, taking the 90th percentile jump in ERA5 from 1960-1990 at each grid point as the jump threshold for that grid point.

Summertime temperature jumps in ERA5 from 1940-2024 (Figure 6a) are more frequent over the Northern Hemisphere midlatitudes, though this is rather noisy due the low number of historical samples. In most regions in the observational record, it is more likely that a jump does not occur, i.e. the default class is "no jump". However, there some locations where jumps are more likely than not (e.g. Southwest Australia) so we also plot the skill that can be achieved by a naive classifier that only predicts the class that is most common in ERA5 at each grid point (Figure 6b). Figure 6b is therefore calculated as max(Figure 6a, 1-Figure 6a)).

In most regions in the observational record, it is more likely that a jump does not occur (i.e., the default class is "no jump"). However, there are some locations where jumps are more likely than not (e.g., Southwest Australia), so we also plot the skill that can be achieved by a naive classifier that only predicts the class that is most common in ERA5 at each grid point (Figure 6b). Figure 6b is therefore calculated as max(Figure 6a, 1-Figure 6a).

We show the CNN accuracy in predicting observed summertime warming jumps in Figure 6c, and the percentage difference in accuracy from random chance in Figure 6e. We see that the CNN largely has poor skill. In places with zero difference in skill between the background likelihood and the CNN skill, the CNN defaults to only predicting "no jump", implying that at no point in the historical record was the warming trend large enough for the CNN to confidently predict that a jump would occur. This finding highlights an interesting point that greenhouse gas warming enhances the predictive skill of summertime warming jumps, but this "emergence" of predictive skill has not occurred in many regions in the historical record. Conversely, places where the CNN does show significant skill above random

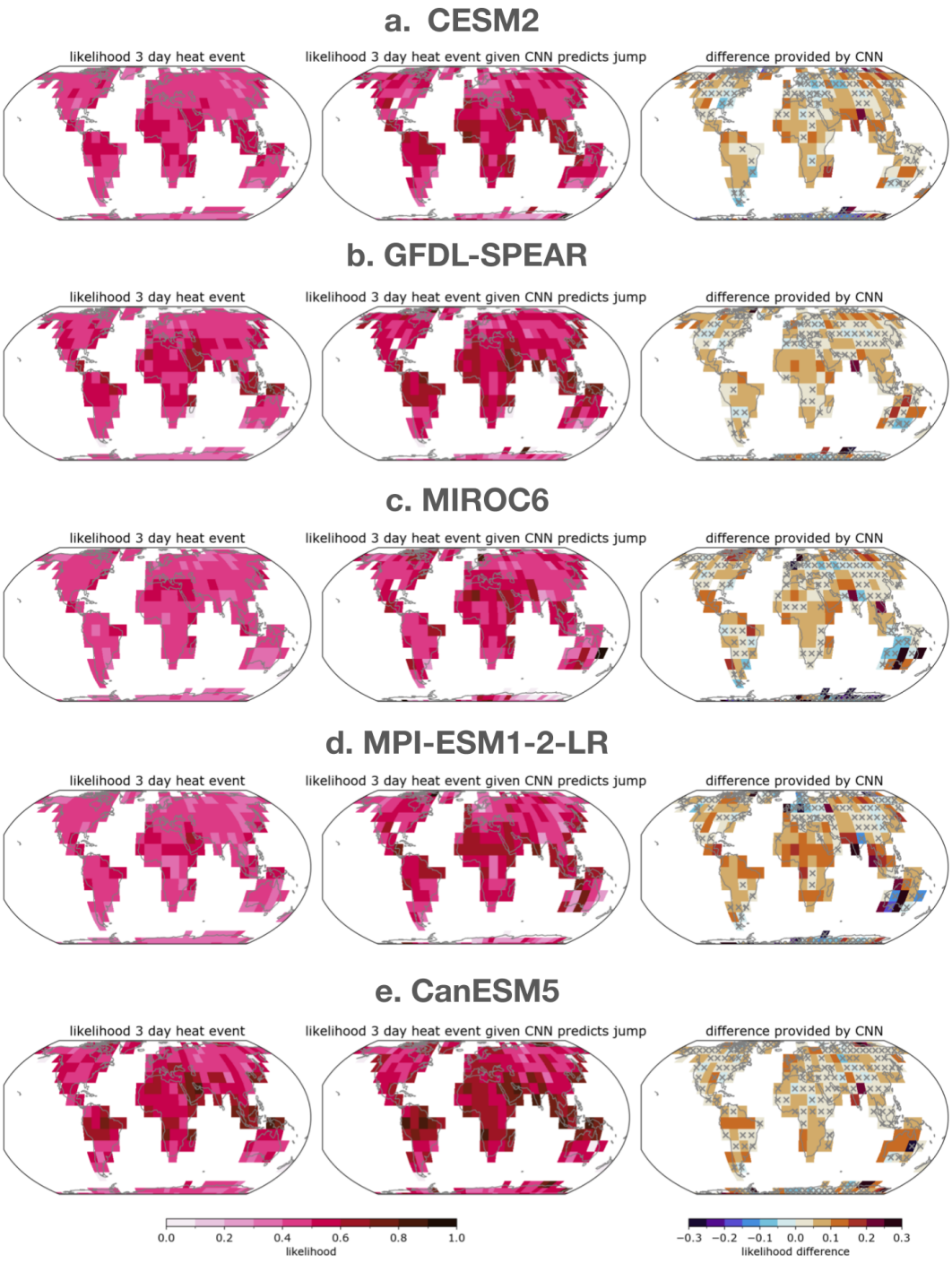

Figure 5. Likelihood in detecting a future 3-day-heat event in individual GCMs. From top to bottom: CESM2, GFDL-SPEAR, MIROC6, MPI-ESM1-2-LR, CanESM5. (Note that we exclude ACCESS-ESM1-5 in this analysis as daily maximum temperatures were not available for all members.) Left column is the frequency of three-day heat event occurrence in the testing members of each GCM large ensemble. Middle column is the likelihood that a three-day heat event occurs given the CNN predicts a warming jump. Right column is the difference between the middle and left-hand columns, demonstrating the increase in detection of a three-day heat event that the CNN's jump predictions provide above random chance.

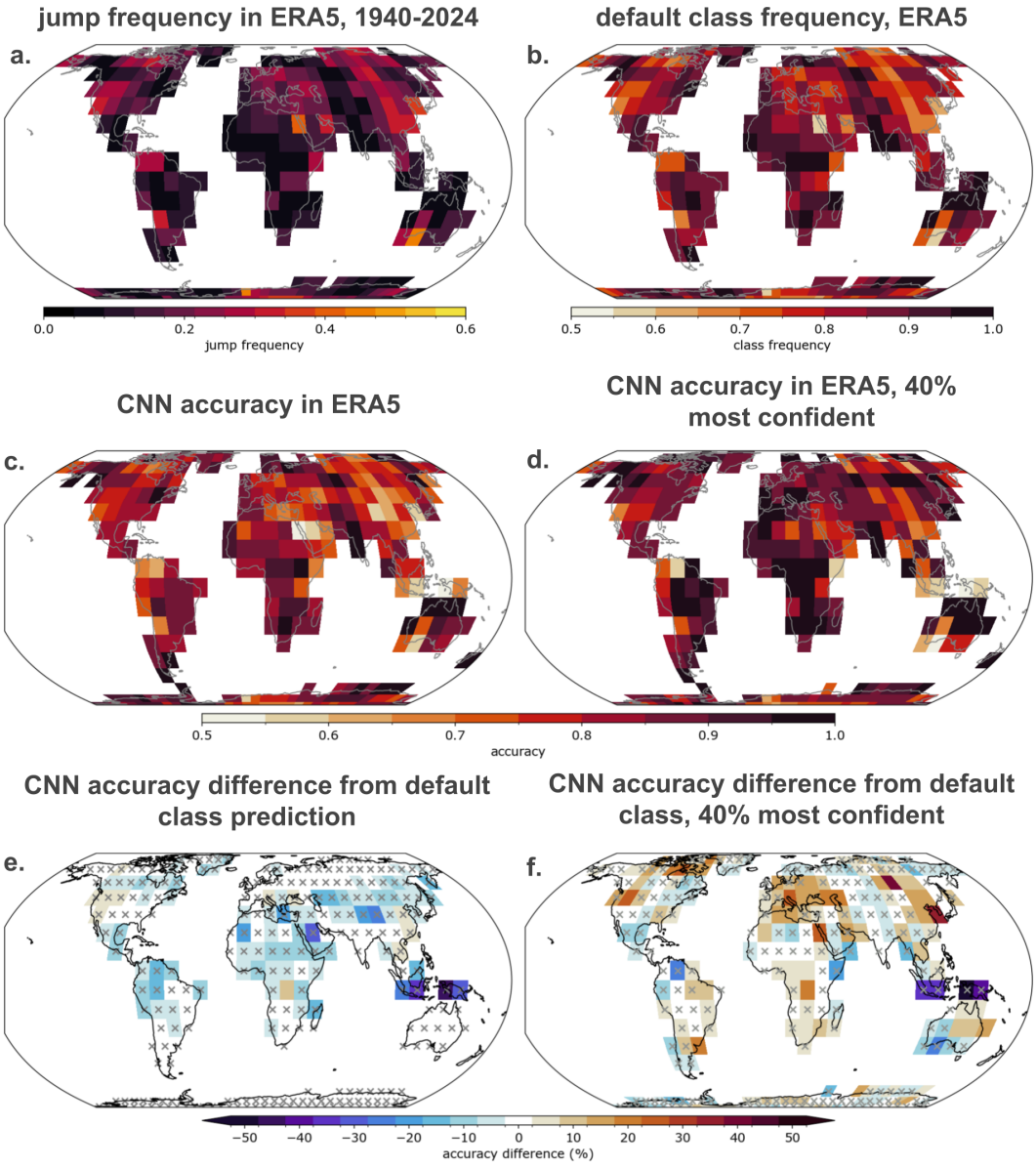

Figure 6. a. Frequency of summertime warming jumps in the observational record, defined as the number of summertime jumps that occur at a grid point divided by the number of years. b. Frequency of the default class in ERA5, defined as the number of no jump summers divided by total years. c. CNN accuracy in predicting summertime jumps in ERA5 when ERSST is used as input data. d. CNN accuracy in predicting summertime jumps in ERA5 for the 40% predictions assigned the highest confidence at each grid point. e. Percentage difference between CNN prediction skill (c.) and random chance (b.). f. Percentage difference between CNN's most confident predictions (d.) and random chance (b.). In panels e. and f., Significance is calculated by randomly resampling 40% of samples from the observational record 100 times and calculating the skill of predicting "no jump" on these selected samples. Skill is significantly improved relative to random chance if CNN accuracy on its 40% most confident samples is greater than the 95% percentile accuracy achieved from the bootstrapped accuracy distribution. x stippling represents grid points where accuracy increase from CNN is not statistically significant at 95%.

guessing in the historical period implies that the warming trend has been large enough for summertime warming jumps to begin to be predictable.

We further examine whether the CNN has learned to distinguish predictable samples in the observational record using the CNN's most confident predictions in observations (Figure 6d), as well as the percentage accuracy difference from random chance of the most confident samples (Figure 6f). In analyzing the CNN's most confident predictions in observations, we include the 40% most confident samples. We choose a lower confidence threshold here because there are only 68 samples in the observational record, and therefore the 40% threshold leaves 27 samples over which to calculate statistical significance. We find grid points with a statistically significant increase in accuracy above random chance, particularly in the Northern Hemisphere midlatitudes (Figure 6f). In these cases, the CNN has largely learned when to be most confident in its prediction of "no jump" occurring. While this category may be less useful for predicting a future extreme, the result does imply that oceanic patterns learned from the GCM data have helped the CNN learn predictable patterns of suppressed summertime warming in the observational record.

4. Discussion & Conclusions

In this study, we have explored the predictability of jumps in summertime average temperatures for a future five-year period. We chose this predicted outcome because these jumps coincide with an increased likelihood of experiencing a 3-day heat extreme. Such short-lived, extreme heat events are themselves not predictable beyond a few weeks when the required atmospheric conditions can be accurately forecasted by numerical weather prediction models. We identify an abrupt jump in average summertime temperature as a covariate of extreme summertime temperatures, and then show that these jumps can be predictable by CNNs trained on large single-model ensembles of global climate model simulations. We further demonstrate that the CNN's summertime jumps predictions also result in enhanced likelihood in detecting a future 3-heat event. Prior studies have demonstrated the linkage between North Atlantic SST variability and the predictability of summertime heat extremes in the Europe-Mediterranean region [Borchert et al., 2019; Wallberg et al., 2024; Mascolo et al., 2025]. This current study demonstrates the linkage between SST variability and predictable regional extreme summertime temperatures across the global land surface, providing a methodology for objectively identifying regions where SST variability contributes to the predictability of summertime temperature extremes beyond the well-studied European region.

Our analyses demonstrate that the prediction skill of a future summer warming jump is improved by conditioning a prediction on the the prior 10-year SST variability. Figure 3 shows skill increases when the prior 10-year SST variability information is incorporated across all samples in the testing set. We also identify substantial skill increases attributable to SST variability when we examine the most confident samples. This "windows of opportunity" approach [Mariotti et al., 2020], where prediction skill is evaluated on the most confidently predicted samples, aligns with the results of Gordon et al. [2023], where it was also shown that the inclusion of recent variability to a neural network's prediction substantially increases its ability to identify windows of opportunity, even in a relatively high climate forcing scenario. While our study has a similar approach to that of Gordon et al. [2023], this current methodology does not require prior exact knowledge of the climate change forced response, meaning that the observational record (where the forced response is not known) can be input without any need for trend removal.

Our results identify regions where summertime warming jumps are most likely to be

predictable in a future climate. One such region is the tropics, where we posit that the skill is largely due to ENSO as the primary driver of regional interannual variability. By inspecting the SST patterns that most frequently result in confident jump predictions, we also find North Pacific Gyre circulation and North Atlantic heat transport also frequently co-occur with confident jump predictions (Figure S7 and S8). Therefore it may also be that the combined mechanisms make summertime warming jumps more likely to occur. A more comprehensive back-tracing of SST patterns contributing to confident predictions is an avenue for future work.

The CNNs also show distinct skill over the Northern Hemisphere extra-tropics, particularly over West Asia, East Asia and the Southwest United States. These patterns of skill resemble those found in prior work for predicting future 1-5 year boreal summertime near-surface temperature extremes in historical observations [Befort and Kruschke, 2025]. Combined, these results imply that there is some interannual predictability in summertime temperature extremes in these regions. Our method in particular reveals that it is not just the forced response to warming that provides predictability in summertime temperature extremes, and prediction skill may also be driven by large-scale ocean variability. However, these results are only one example of identifying summertime temperature predictability, and other methods are very likely to improve on the skill identified here. We also acknowledge that our methodology does not account for local vulnerability to heat extremes, and therefore future work should look to identify the patterns of large-scale variability that lead to confident predictions, with a specific focus on regions where climatological and socioeconomic factors amplify the consequences of heat extremes.

One limitation of this study is the use of GCM data for training and verification of the CNNs. While we have been able to show, in a perfect model set-up, that future summertime warming jumps are predictable beyond the change of frequency with climate change, it is less clear how well this predictability translates to predicting such events in observations. We show that the CNN has some ability to predict the observational record; in particular it appears that the CNNs have learned some oceanic patterns that are more likely to predictably suppress summertime temperature jumps. We also observe predictive skill of summertime warming jumps in places such as the tropics where the climate change signal provides a larger fraction of temperature variability. This evidence suggests that the CNNs are able to learn climate signals from GCM data that are relevant for predicting land surface temperature change on multi-year timescales, a result that has been reported elsewhere for oceanic variability, and shorter-timescale variability [Davenport et al., 2024; Gibson et al., 2021]. Training machine learning models on GCM data is therefore a powerful tool for climate prediction research, with the caveat that GCMs represent imperfect approximations of the Earth system and may contain unknown biases. Approaches such as transfer learning may make machine learning models more faithful to the observed Earth System [Immorlano et al., 2025; Barnes et al., 2025], but they come at the expense of statistical robustness as the methodology incorporates observational data into the training stage, leaving little independent observational data with even fewer degrees of freedom for independent testing.

The simulations in this study do not include volcanic eruptions in their future projections. This exclusion means that we cannot test the CNNs' ability to predict summertime warming jumps that may follow the short-lived cooling of a future Pinatubo-like eruption. While there is an uptick in summertime warming jumps following Pinatubo in both the GCM historical simulations and in the observational record, it appears that the CNNs' predictions of these jumps is delayed by 2-3 years (Figure S9). The CNNs are not provided with the simulation year, so this delay is likely due to the CNN detecting the abrupt cooling in the

years following Pinatubo in the input data. There is however no clear signature of an uptick in jump predictions in observations, so we cannot conclude whether the CNNs have learned a generalizable signature of volcanic activity, or if it is has learned the exact Pinatubo response in each of simulations (which is a forcing included in every training and validation member).

The jump threshold used in this work was specifically chosen to be relative to recently experienced warming. We chose this definition because a summertime warming jump in a future, warmer, climate is still a jump above the recently experienced warming at the time that the jump occurs. If we consider a future with some adaptation to recent warming (e.g., adoption of air conditioning, more available cooling centers, etc.), the summertime jump exemplifies an event that could strain recent adaptive measures, and therefore the prediction of such an event could identify imminent risks and inform near-term adaptive measures. We therefore encourage future work to examine extreme event prediction in the context of recently experienced warming, rather than only from a past historical baseline.

Our framing of extreme event predictability with contributions from both external forcing and internal variability highlights that extreme events, which become more frequent with increasing warming, also become more predictable, and that this predictability has not emerged everywhere in the observational record. While this is a departure from the established paradigm that global warming provides no predictability because it is a deterministic signal [DelSole and Tippett, 2018], we believe that it is still important to quantify when events that cause extreme stress on human and natural systems become more predictable as they become more frequent. Identifying the emergence of predictability of extreme events should thus be a priority for future work.

Near-term regional extreme event prediction is a multi-faceted challenge – the events themselves are rare, the historical data record is short and their physical mechanisms span the ocean, atmosphere and land systems. Such a challenge requires a multi-faceted solution. Here we leverage recent advances in machine learning and climate modeling to develop a framework for approaching this challenge. Our application of this framework to the prediction of multi-day extreme heat events reveals, along with other recent work [Borchert et al., 2019; Solaraju-Murali et al., 2021; Lockwood et al., 2023], suggests that extreme event prediction can be enhanced by hypothesis-based approaches that relate our understanding of predictable large-scale variability to climate indicators that lead to enhanced frequency of extreme events.

Code & Data Availability

GCM data is available from the Earth System Grid Federation (ESGF) https://aims2.llnl.gov/search, except for the CESM2 Large Ensemble which available from the NCAR Research Data archive https://rda.ucar.edu/datasets/d651056/dataaccess/, and GFDL-SPEAR-MED data which is available at https://noaa-gfdl-spear-large-ensembles-pds.s3.amazonaws.com/index.html#SPEAR/GFDL-LARGE-ENSEMBLES/CMIP/NOAA-GFDL/GFDL-SPEAR-MED/. ERA5 data was downloaded from https://cds.climate.copernicus.eu/datasets/reanalysis-era5-single-levels-monthly-means?tab=overview, ERSST from https://psl.noaa.gov/data/gridded/data.noaa.ersst.v5.html, and HadCRUT5 with anomalies and absolute values from https://crudata.uea.ac.uk/cru/data/temperature/. Code is available at

Acknowledgments

We would like to thank the Stanford Doerr School Center for Computation and the Stanford Research Computing Center for providing computational resources. We acknowledge financial support from Stanford Data Science and Stanford University

References

Arblaster, J. M. and Alexander, L. V. (2012). The impact of the El Niño-Southern Oscillation on maximum temperature extremes. *Geophysical Research Letters*, 39(20).

Barnes, E. A., Diffenbaugh, N. S., and Seneviratne, S. I. (2025). Combining climate models and observations to predict the time remaining until regional warming thresholds are reached. *Environ. Res. Lett.*, 20(1):014008.

Becker, E. J., van den Dool, H., and Peña, M. (2013). Short-term climate extremes: Prediction skill and predictability. *J. Clim.*, 26(2):512–531.

Befort, D. J. and Kruschke, T. (2025). Decadal prediction of the probability of extreme seasons. *Environ. Res. Lett.*, 20(5):054054.

Boer, G. J., Smith, D. M., Cassou, C., Doblas-Reyes, F., Danabasoglu, G., Kirtman, B., Kushnir, Y., Kimoto, M., Meehl, G. A., Msadek, R., Mueller, W. A., Taylor, K. E., Zwiers, F., Rixen, M., Ruprich-Robert, Y., and Eade, R. (2016). The Decadal Climate Prediction Project (DCPP) contribution to CMIP6. *Geosci. Model Dev.*, 9(10):3751–3777.

Borchert, L. F., Pohlmann, H., Baehr, J., Neddermann, N.-C., Suarez-Gutierrez, L., and Müller, W. A. (2019). Decadal predictions of the probability of occurrence for warm summer temperature extremes. *Geophys. Res. Lett.*, 46(23):14042–14051.

Davenport, F. V., Barnes, E. A., and Gordon, E. M. (2024). Combining neural networks and CMIP6 simulations to learn windows of opportunity for skillful prediction of multiyear sea surface temperature variability. *Geophys. Res. Lett.*, 51(11):e2023GL108099.

Delgado-Torres, C., Donat, M. G., Soret, A., González-Reviriego, N., Bretonnière, P.-A., Ho, A.-C., Pérez-Zanón, N., Cabré, M. S., and Doblas-Reyes, F. J. (2023). Multi-annual predictions of the frequency and intensity of daily temperature and precipitation extremes. *Environ. Res. Lett.*, 18(3):034031.

DelSole, T. and Tippett, M. K. (2018). Predictability in a changing climate. *Clim. Dyn.*, 51(1):531–545.

Delworth, T. L., Cooke, W. F., Adcroft, A., Bushuk, M., Chen, J.-H., Dunne, K. A., Ginoux, P., Gudgel, R., Hallberg, R. W., Harris, L., Harrison, M. J., Johnson, N., Kapnick, S. B., Lin, S.-J., Lu, F., Malyshev, S., Milly, P. C., Murakami, H., Naik, V., Pascale, S., Paynter, D., Rosati, A., Schwarzkopf, M. D., Shevliakova, E., Underwood, S., Wittenberg, A. T., Xiang, B., Yang, X., Zeng, F., Zhang, H., Zhang, L., and Zhao, M. (2020). SPEAR: The next generation GFDL modeling system for seasonal to multidecadal prediction and projection. *J. Adv. Model. Earth Syst.*, 12(3).

Dunstone, N., Lockwood, J., Solaraju-Murali, B., Reinhardt, K., Tsartsali, E. E., Athanasiadis, P. J., Bellucci, A., Brookshaw, A., Caron, L.-P., Doblas-Reyes, F. J., Früh, B., González-Reviriego, N., Gualdi, S., Hermanson, L., Materia, S., Nicodemou, A., Nicolì, D., Pankatz, K., Paxian, A., Scaife, A., Smith, D., and Thornton, H. E. (2022). Towards Useful Decadal Climate Services. *Bull. Am. Meteorol. Soc.*, 103(7):E1705–E1719.

Eade, R., Hamilton, E., Smith, D. M., Graham, R. J., and Scaife, A. A. (2012). Forecasting the number of extreme daily events out to a decade ahead. *Journal of Geophysical Research: Atmospheres*, 117(D21).

Eade, R., Smith, D., Scaife, A., Wallace, E., Dunstone, N., Hermanson, L., and Robinson, N. (2014). Do seasonal-to-decadal climate predictions underestimate the predictability of the real world? *Geophys. Res. Lett.*, 41(15):5620–5628.

Ebi, K. L., Hasegawa, T., Hayes, K., Monaghan, A., Paz, S., and Berry, P. (2018). Health risks of warming of 1.5 °C, 2 °C, and higher, above pre-industrial temperatures. *Environ. Res. Lett.*, 13(6):063007.

Field, C. B., Barros, V., Stocker, T. F., and Dahe, Q., editors (2012). *Managing the risks of extreme events and disasters to advance climate change adaptation: special report of the Intergovernmental Panel on Climate Change*. Cambridge University Press, Cambridge, England.

Fischer, E. M., Sippel, S., and Knutti, R. (2021). Increasing probability of record-shattering climate extremes. *Nat. Clim. Chang.*, 11(8):689–695.

Gibson, P. B., Chapman, W. E., Altinok, A., Delle Monache, L., DeFlorio, M. J., and Waliser, D. E. (2021). Training machine learning models on climate model output yields skillful interpretable seasonal precipitation forecasts. *Communications Earth & Environment*, 2(1):1–13.

Gordon, E. M., Barnes, E. A., and Davenport, F. V. (2023). Separating internal and forced contributions to near term SST predictability in the CESM2-LE. *Environ. Res. Lett.*, 18(10):104047.

Gordon, E. M. and Diffenbaugh, N. S. (2025). Identifying a Pattern of Predictable Decadal North Pacific SST Variability in Historical Observations. *Geophysical Research Letters*, 52(5):e2024GL112729.

Hawkins, E. and Sutton, R. (2009). The Potential to Narrow Uncertainty in Regional Climate Predictions. *Bull. Am. Meteorol. Soc.*, 90(8):1095–1108.

He, Y., Wang, B., Li, L., Liu, J., Wang, Y., and Li, F. (2022). Role of Ocean Initialization in Skillful Prediction of Sahel Rainfall on the Decadal Timescale. *J. Clim.*, -1(aop):1–43.

Hersbach, H., Bell, B., Berrisford, P., Hirahara, S., Horányi, A., Muñoz-Sabater, J., Nicolas, J., Peubey, C., Radu, R., Schepers, D., Simmons, A., Soci, C., Abdalla, S., Abellan, X., Balsamo, G., Bechtold, P., Biavati, G., Bidlot, J., Bonavita, M., De Chiara, G., Dahlgren, P., Dee, D., Diamantakis, M., Dragani, R., Flemming, J., Forbes, R., Fuentes, M., Geer, A., Haimberger, L., Healy, S., Hogan, R. J., Hólm, E., Janisková, M., Keeley, S., Laloyaux, P., Lopez, P., Lupu, C., Radnoti, G., de Rosnay, P., Rozum, I., Vamborg, F., Villaume, S., and Jean-Noël Thépaut (2020). The ERA5 global reanalysis. *Q. J. R. Meteorol. Soc.*, 146(730):1999–2049.

Immorlano, F., Eyring, V., le Monnier de Gouville, T., Accarino, G., Elia, D., Mandt, S., Aloisio, G., and Gentine, P. (2025). Transferring climate change physical knowledge. *Proc. Natl. Acad. Sci. U. S. A.*, 122(15):e2413503122.

Lehner, F., Deser, C., Maher, N., Marotzke, J., Fischer, E. M., Brunner, L., Knutti, R., and Hawkins, E. (2020). Partitioning climate projection uncertainty with multiple large ensembles and CMIP5/6. *Earth Syst. Dyn.*, 11(2):491–508.

Lockwood, J. F., Dunstone, N., Hermanson, L., Saville, G. R., Scaife, A. A., Smith, D., and Thornton, H. E. (2023). A decadal climate service for insurance: Skilful multi-

year predictions of North Atlantic hurricane activity and US hurricane damage. *J. Appl. Meteorol. Climatol.*, -1(aop).

Luo, M. and Lau, N.-C. (2020). Summer heat extremes in northern continents linked to developing ENSO events. *Environ. Res. Lett.*, 15(7):074042.

Mariotti, A., Baggett, C., Barnes, E. A., Becker, E., Butler, A., Collins, D. C., Dirmeyer, P. A., Ferranti, L., Johnson, N. C., Jones, J., Kirtman, B. P., Lang, A. L., Molod, A., Newman, M., Robertson, A. W., Schubert, S., Waliser, D. E., and Albers, J. (2020). Windows of Opportunity for Skillful Forecasts Subseasonal to Seasonal and Beyond. *Bull. Am. Meteorol. Soc.*, 101(5):E608–E625.

Mascolo, V., Le Priol, C., D'Andrea, F., and Bouchet, F. (2025). Comparing the influence of atlantic multidecadal variability and spring soil moisture on european summer heat waves. *Oxf. Open Clim. Chang.*, 5(1):kgae023.

Mayer, K. J. and Barnes, E. A. (2021). Subseasonal Forecasts of Opportunity Identified by an Explainable Neural Network. *Geophys. Res. Lett.*, 48(10):e2020GL092092.

McGovern, A., Lagerquist, R., Gagne, D. J., Eli Jergensen, G., Elmore, K. L., Homeyer, C. R., and Smith, T. (2019). Making the Black Box More Transparent: Understanding the Physical Implications of Machine Learning. *Bull. Am. Meteorol. Soc.*, 100(11):2175–2199.

Meehl, G. A., Richter, J. H., Teng, H., Capotondi, A., Cobb, K., Doblas-Reyes, F., Donat, M. G., England, M. H., Fyfe, J. C., Han, W., Kim, H., Kirtman, B. P., Kushnir, Y., Lovenduski, N. S., Mann, M. E., Merryfield, W. J., Nieves, V., Pegion, K., Rosenbloom, N., Sanchez, S. C., Scaife, A. A., Smith, D., Subramanian, A. C., Sun, L., Thompson, D., Ummenhofer, C. C., and Xie, S.-P. (2021). Initialized Earth System prediction from subseasonal to decadal timescales. *Nature Reviews Earth & Environment*, 2(5):340–357.

Meehl, G. A., Senior, C. A., Eyring, V., Flato, G., Lamarque, J.-F., Stouffer, R. J., Taylor, K. E., and Schlund, M. (2020). Context for interpreting equilibrium climate sensitivity and transient climate response from the CMIP6 Earth system models. *Sci. Adv.*, 6(26):eaba1981.

Meehl, G. A., Teng, H., Smith, D., Yeager, S., Merryfield, W., Doblas-Reyes, F., and Glanville, A. A. (2022). The effects of bias, drift, and trends in calculating anomalies for evaluating skill of seasonal-to-decadal initialized climate predictions. *Clim. Dyn.*

Meehl, G. A., Zwiers, F., Evans, J., Knutson, T., Mearns, L., and Whetton, P. (2000). Trends in extreme weather and climate events: Issues related to modeling extremes in projections of future climate change. *Bull. Am. Meteorol. Soc.*, 81(3):427–436.

Morice, C. P., Kennedy, J. J., Rayner, N. A., Winn, J. P., Hogan, E., Killick, R. E., Dunn, R. J. H., Osborn, T. J., Jones, P. D., and Simpson, I. R. (2021). An updated assessment of near-surface temperature change from 1850: The HadCRUT5 data set. *J. Geophys. Res.*, 126(3):e2019JD032361.

Olonscheck, D., Suarez-Gutierrez, L., Milinski, S., Beobide-Arsuaga, G., Baehr, J., Fröb, F., Ilyina, T., Kadow, C., Krieger, D., Li, H., Marotzke, J., Plésiat, E., Schupfner, M., Wachsmann, F., Wallberg, L., Wieners, K.-H., and Brune, S. (2023). The new Max Planck Institute Grand Ensemble with CMIP6 forcing and high-frequency model output. *J. Adv. Model. Earth Syst.*, 15(10):e2023MS003790.

Rayner, N. A., Parker, D. E., Horton, E. B., Folland, C. K., Alexander, L. V., Rowell, D. P., Kent, E. C., and Kaplan, A. (2003). Global analyses of sea surface temperature, sea ice, and night marine air temperature since the late nineteenth century. *Journal of Geophysical Research: Atmospheres*, 108(4407).

Rodgers, K. B., Lee, S.-S., Rosenbloom, N., Timmermann, A., Danabasoglu, G., Deser, C., Edwards, J., Kim, J.-E., Simpson, I. R., Stein, K., Stuecker, M. F., Yamaguchi, R., Bódai, T., Chung, E.-S., Huang, L., Kim, W. M., Lamarque, J.-F., Lombardozzi, D. L., Wieder, W. R., and Yeager, S. G. (2021). Ubiquity of human-induced changes in climate variability. *Earth Syst. Dyn.*, 12(4):1393–1411.

Rupp, D. E., Li, S., Mote, P. W., Massey, N., Sparrow, S. N., and Wallom, D. C. H. (2017). Influence of the ocean and greenhouse gases on severe drought likelihood in the central United States in 2012. *J. Clim.*, 30(5):1789–1806.

Seneviratne, S. I., Zhang, X., Adnan, M., Badi, W., Dereczynski, C., Luca, A. D., Ghosh, S., Iskandar, I., Kossin, J., Lewis, S., Otto, F., Pinto, I., Satoh, M., Vicente-Serrano, S. M., Wehner, M., Zhou Masson-Delmotte, B., Zhai, P., Pirani, A., Connors, S. L., Péan, C., Berger, S., Caud, N., Chen, Y., Goldfarb, L., Gomis, M. I., Huang, M., Leitzell, K., Lonnoy, E., Matthews, J. B. R., Maycock, T. K., Waterfield, T., Yelekçi, O., Yu, R., and Zhou, B. (2021). Chapter 11: Weather and Climate Extreme Events in a Changing Climate. In *Climate Change 2021: The Physical Science Basis. Contribution of Working Group I to the Sixth Assessment Report of the Intergovernmental Panel on Climate Change*. Cambridge University Press, Cambridge, United Kingdom; New York, NY, USA.

Smith, D. M., Eade, R., Scaife, A. A., Caron, L.-P., Danabasoglu, G., DelSole, T. M., Delworth, T., Doblas-Reyes, F. J., Dunstone, N. J., Hermanson, L., Kharin, V., Kimoto, M., Merryfield, W. J., Mochizuki, T., Müller, W. A., Pohlmann, H., Yeager, S., and Yang, X. (2019). Robust skill of decadal climate predictions. *npj Climate and Atmospheric Science*, 2(1):1–10.

Solaraju-Murali, B., Gonzalez-Reviriego, N., Caron, L.-P., Ceglar, A., Toreti, A., Zampieri, M., Bretonnière, P.-A., Samsó Cabré, M., and Doblas-Reyes, F. J. (2021). Multi-annual prediction of drought and heat stress to support decision making in the wheat sector. *npj Climate and Atmospheric Science*, 4(1):1–9.

Swart, N. C., Cole, J. N. S., Kharin, V. V., Lazare, M., Scinocca, J. F., Gillett, N. P., Anstey, J., Arora, V., Christian, J. R., Hanna, S., Jiao, Y., Lee, W. G., Majaess, F., Saenko, O. A., Seiler, C., Seinen, C., Shao, A., Sigmond, M., Solheim, L., von Salzen, K., Yang, D., and Winter, B. (2019). The Canadian Earth System Model version 5 (CanESM5.0.3). *Geosci. Model Dev.*, 12(11):4823–4873.

Tatebe, H., Ogura, T., Nitta, T., Komuro, Y., Ogochi, K., Takemura, T., Sudo, K., Sekiguchi, M., Abe, M., Saito, F., Chikira, M., Watanabe, S., Mori, M., Hirota, N., Kawatani, Y., Mochizuki, T., Yoshimura, K., Takata, K., O'ishi, R., Yamazaki, D., Suzuki, T., Kurogi, M., Kataoka, T., Watanabe, M., and Kimoto, M. (2019). Description and basic evaluation of simulated mean state, internal variability, and climate sensitivity in MIROC6. *Geosci. Model Dev.*, 12(7):2727–2765.

Trenberth, K. E., Fasullo, J. T., and Shepherd, T. G. (2015). Attribution of climate extreme events. *Nat. Clim. Chang.*, 5(8):725–730.

Wallberg, L., Suarez-Gutierrez, L., Matei, D., and Müller, W. A. (2024). Extremely warm european summers preceded by sub-decadal north atlantic ocean heat accumulation. *Earth Syst. Dyn.*, 15(1):1–14.

Wei, W., Yan, Z., and Li, Z. (2021). Influence of Pacific Decadal Oscillation on global precipitation extremes. *Environ. Res. Lett.*, 16(4):044031.

White, R. H., Anderson, S., Booth, J. F., Braich, G., Draeger, C., Fei, C., Harley, C. D. G., Henderson, S. B., Jakob, M., Lau, C.-A., Mareshet Admasu, L., Narinesingh, V., Rodell, C.,

Roocroft, E., Weinberger, K. R., and West, G. (2023). The unprecedented Pacific Northwest heatwave of June 2021. *Nat. Commun.*, 14(1):727.

Zhang, W. and Kirtman, B. (2019). Understanding the signal-to-noise paradox with a simple Markov model. *Geophys. Res. Lett.*, 46(22):13308–13317.

Ziehn, T., Chamberlain, M. A., Law, R. M., Lenton, A., Bodman, R. W., Dix, M., Stevens, L., Wang, Y.-P., and Srbinovsky, J. (2020). The Australian Earth System Model: ACCESS-ESM1.5. *JSHESS*, 70(1):193–214.